Received: 20 August 2021 | Revised: 5 January 2022 | Accepted: 29 January 2022

DOI: 10.1111/ina.13000

ORIGINAL ARTICLE

WILEY

Modeling and experimental study of dispersion and deposition of respiratory emissions with implications for disease transmission

Simon Coldrick[1] | Adrian Kelsey[1] | Matthew J. Ivings[1] | Timothy G. Foat[2] | Simon T. Parker[2] | Catherine J. Noakes[3] | Allan Bennett[4] | Helen Rickard[4] | Ginny Moore[4]

[1]Health and Safety Executive, Buxton, Derbyshire, UK

[2]Defence Science and Technology Laboratory, Salisbury, UK

[3]Leeds Institute for Fluid Dynamics, School of Civil Engineering, University of Leeds, Leeds, UK

[4]National Infection Service, UKHSA, Salisbury, UK

Correspondence
Simon Coldrick, Health and Safety Executive, Harpur Hill, Buxton, Derbyshire, SK17 9JN, UK.
Email: simon.coldrick@hse.gov.uk

Funding information
PROTECT, the National Core Study on Transmission and the Environment

Abstract

The ability to model the dispersion of pathogens in exhaled breath is important for characterizing transmission of the SARS-CoV-2 virus and other respiratory pathogens. A Computational Fluid Dynamics (CFD) model of droplet and aerosol emission during exhalations has been developed and for the first time compared directly with experimental data for the dispersion of respiratory and oral bacteria from ten subjects coughing, speaking, and singing in a small unventilated room. The modeled exhalations consist of a warm, humid, gaseous carrier flow and droplets represented by a discrete Lagrangian particle phase which incorporates saliva composition. The simulations and experiments both showed greater deposition of bacteria within 1 m of the subject, and the potential for a substantial number of bacteria to remain airborne, with no clear difference in airborne concentration of small bioaerosols (<10 μm diameter) between 1 and 2 m. The agreement between the model and the experimental data for bacterial deposition directly in front of the subjects was encouraging given the uncertainties in model input parameters and the inherent variability within and between subjects. The ability to predict airborne microbial dispersion and deposition gives confidence in the ability to model the consequences of an exhalation and hence the airborne transmission of respiratory pathogens such as SARS-CoV-2.

KEYWORDS
computational fluid dynamics, exhalation, microorganism, respiratory, SARS-CoV-2

Funding information PROTECT, the National Core Study on Transmission and the Environment.

1 | INTRODUCTION

The SARS-CoV-2 pandemic has brought about the need to assess the risks posed by different viral and bacterial transmission routes for hazardous respiratory infections. Knowledge of the relative importance of these different routes is important in understanding the ways in which infection can be transmitted and in determining the best combination of control measures. The two main routes of infectious disease transmission are contact or airborne. Contact transmission may be by direct contact with droplets from a contaminated individual or indirect contact such as touching a contaminated surface (fomite transmission). Airborne transmission arises from pathogen-laden exhaled aerosols which are inhaled.[1] Droplets and aerosols exhaled during normal activities (breathing, talking, singing, coughing, and sneezing) have a range of diameters from <1 μm to >100 μm, and this plays an important role in the routes by which infection could occur. Very large droplets (>100 μm), which may be able to carry a larger microbial load, typically follow a ballistic trajectory and are unlikely to fully evaporate before they deposit on surfaces or on a susceptible individual. Those in smaller diameter ranges experience, proportionally, increased evaporation[2] with a final diameter depending on their initial size and respiratory fluid composition.[3] Studies have suggested[4,5] that the microbial load depends on droplet size and origin, though these relationships remain uncertain and may vary with the type of bacteria or virus. However, the smallest aerosols may be more numerous than large droplets, may remain suspended in the air for relatively long periods, and can be inhaled by a susceptible individual. It is also recognized that dispersion behavior is heavily affected by environmental factors and there is no absolute distinction between the fate of large droplets and aerosols, that is, there is a continuum of behavior across the spectrum of diameters. The mechanism of airborne transmission has long been acknowledged[6] and plays an important role in the spread of multiple infectious diseases including bacterial pathogens such as tuberculosis,[7] and viral diseases including measles,[8] influenza,[9] and SARS.[10] The World Health Organisation (WHO) recently acknowledged the role of airborne routes in the transmission of SARS-CoV-2.[11]

Characterization of the range of droplet and aerosol sizes in exhaled breath and their effect on transmission has long been recognized as an important part of understanding the transmission of infection. Early work to characterize the size distribution of exhaled droplets by Duguid[12] demonstrated significantly greater numbers of droplets (and correspondingly much greater volumes of fluid) are released during sneezing and coughing compared to talking. More recent investigations (Johnson et al.,[13] Gregsonet al.,[14]), demonstrate a wide variation in the number and size of with different vocal activities and between different people. There have also been a number of studies to characterize exhalation flows,[15,16] which are an important part of defining the initial air movement from the mouth and nose which propel and carry the respiratory droplets and aerosols.

Mathematical modeling can help provide insight into the physics of transmission. Droplet evaporation models, (for example Chen et al.,[17] de Oliveira et al.,[18] Wei and Li,[19] Xie et al.,[2] Walker et al.,[20]), can be used to explore the influence of environmental factors such as relative humidity, temperature, and diameter change due to evaporation which can influence how droplets behave. One of the limitations of these models is that they are unable to account for factors such as ventilation flows which can influence the transport and deposition of airborne droplets. Other types of models, such as Noakes and Sleigh,[21] Burridge et al.,[22] or Jones et al.,[23] consider transmission risks as a function of ventilation and pathogen emission rates, but without explicitly modeling the transport and evaporation of droplets.

Computational Fluid Dynamics provides a means of modeling both the droplet physics and the effects of ventilation and can model realistic geometries and their effect on the flow. CFD has been used to model the transmission of infectious diseases, particularly in relation to the SARS and current SARS-CoV-2 outbreaks (e.g.[24-29]). The main benefit of CFD is that it can combine models to describe the interaction of exhaled droplets with environmental flows that influence the behavior of droplets, such as ventilation and thermal effects. CFD modeling can also be used to understand the effects of mitigation methods such as screens, more complex geometries, or the influence of additional people within the environment.

There are, however, numerous challenges to modeling these scenarios using CFD. Droplets of a few microns size in exhalations can evaporate in less than a few seconds. Furthermore, room geometries may be of the order of several meters in dimension and have air change intervals spanning many minutes. Combining these variables and scales into single simulations means that computer run times can become prohibitively long. A further challenge is that the input conditions or source terms (e.g., for exhalations) need to be defined from the outset and these can have a large influence on the results. Long simulation times can limit the scope of sensitivity analysis that can be carried out on the inputs, and a heavy reliance is made on the strength of input assumptions.

Validation is an important aspect of a modeling study to provide assurance that the assumptions and inputs used in the simulation are appropriate. One of the challenges in validating exhalation models is that the experimental data to cover all aspects from droplet production through transport to deposition, viral load, and infection do not currently exist. For this reason, many previous modeling studies have focussed on validating components of the model as a means of gaining confidence in the overall predictions. A number of studies have compared CFD simulations to exhalation flows from people,[29] idealized experiments with manikins in chambers,[30] and bioaerosol chamber experiments using artificial generation of microbial aerosols from a nebulizer.[31] However, to our knowledge, there are no previous studies that directly compared CFD or droplet model simulation studies with human volunteers exhaling microorganisms.

In the current study, a CFD model of exhalations has been developed and compared to experimental data for surface deposition and air sampling of exhaled bacteria carrying droplets from human participants. The experiments were carried out to quantify the airborne dispersion and deposition of exhaled droplets to provide data for SARS-CoV-2 risk assessments, using detection of respiratory and

oral bacteria as a surrogate for virus-laden droplets. Component validation studies were also carried out on individual elements of the CFD model, such as an exhalation jet and single droplet evaporation, to give confidence in the overall predictions from the model.

2 | INDOOR EXHALATION DISPERSION EXPERIMENTS

Experiments were carried out by the United Kingdom Health Security Agency (UKHSA) to investigate the behavior of exhaled aerosol and droplet particles. The study measured respiratory bacteria as a means of assessing the dispersion characteristics of aerosols and droplets in a 4 x 2.3 x 2.3 m (Length × Width × Height) environmental chamber, shown in Figure 1(A). The chamber was unventilated during experiments, with the only flow provided by air samplers operated during the study.

Ten laboratory workers were recruited to carry out the study, with an age range of 21–59 years and gender balance of 50% female and 50% male. Ethical approval for the study was given by the UKHSA Research Ethics and Governance of Public Health Practice Group (UKHSA REGG). The participants wore hooded Tyvek suits, shoe coverings, and gloves to reduce shedding of non-oral microorganisms and remained seated facing forwards during the study. Participants provided a spit sample into a universal container before each experiment, primarily to assess bacterial load. Participants were seated at one end of the chamber and were required to perform a sequential set of activities as follows: cough three times; read out loud the numbers from 1 to 100; inhale and exhale 3 times; sing happy birthday twice loudly; inhale and snort 3 times; read out loud the numbers from 1 to 100; and cough three times.

Samples were collected by air samplers (Andersen 6 stage and Slit samplers) and on 15 Columbia Blood Agar (CBA) settle plates placed at 20 cm intervals directly in front of and to the side of the subject. The Andersen samplers operated at 28.3 L/min and collected particles onto six CBA plates fractionated by particle diameter, though the breakdown by diameter was not included in the results. The slit samplers sampled onto a rotating CBA plate at the same flow rate. Both samplers were operated for a period of 10 min. Sampler positions are described in the CFD modeling section below. Immediately before the start of the experiment, the settle plates had their lids removed, the air samplers were switched on automatically and the ventilation was turned off remotely. At the end of each 10-min period, the samples were collected and incubated for analysis and the room was ventilated with filtered air for at least 10 min at 180 air changes per hour before the next study.

The number of colony-forming units (CFUs) collected and cultured on each plate was used to define the bacterial deposition onto the surface or the total sampled from the air over the ten-minute experimental period. The type of bacteria and their origin (e.g., organisms from the respiratory tract) that formed the colonies in these assays have not yet been determined. Consequently, a proportion of the colonies detected may have come from other sources.

3 | COMPUTATIONAL FLUID DYNAMICS MODELING OF EXHALATIONS

In line with previous CFD studies,[24,25,27,28,29] the approach adopted for modeling exhalations is the Euler-Lagrange approach. The Eulerian fluid is modeled on a fixed computational mesh through which the flow field is calculated. The Lagrangian method involves computationally tracking the trajectories of individual droplets as a discrete phase, throughout the calculated flow field from their point of introduction until they deposit on a surface or escape the domain. One of the main benefits of this method is that a fixed count of particles having specific diameters can be modeled. Model outputs such as deposited mass can therefore be calculated for use in further analysis such as in a Quantitative Microbial Risk Assessment (QMRA).[32] While other studies[33,34] have used a purely Eulerian drift-flux framework to study size-resolved particle concentration and deposition, such approaches may not be able to capture trajectories for larger droplets with significant inertia.

The simulations in this study were carried out using the commercial software ANSYS Fluent 19.0.[35] The mixture of air, water vapor, and exhaled carbon dioxide in the Eulerian phase was modeled using a species transport model. The local mass fraction of each species was solved for with a convection-diffusion equation which included a source term for the transfer of water vapor from the Lagrangian droplets to the Eulerian phase.

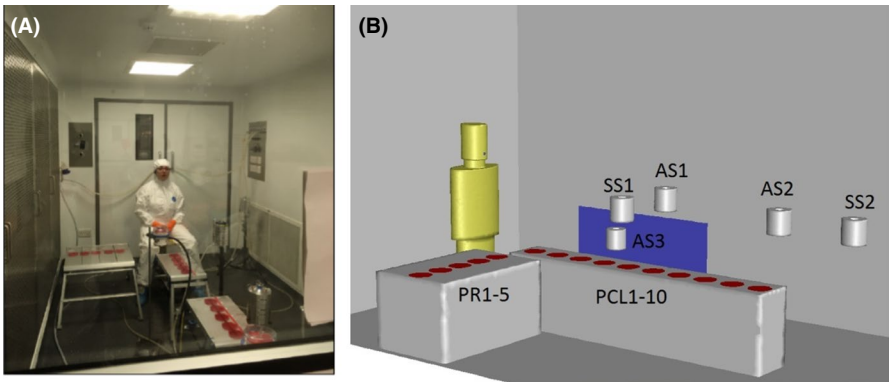

FIGURE 1 (A) Experimental set up in the environmental chamber and modeled geometry (B). The modeled geometry shows the sampler locations with the naming convention used to present the results

3.1 | Geometry and meshing

The modeled geometry is shown in Figure 1(B). The tables holding the settle plates were 0.5 m high and approximated by cuboidal volumes, with the centerline settle plates labeled PCL1-PCL10 and the right hand side settle plates labeled PR1-PR5, with PCL1 and PR1 being closest to the subject. The centerline plates were set out to a distance of 2 m from the subject's assumed knee position, and the right hand plates were set out to 1 m from the subject's assumed knee position. The air samplers, at 1 m height, were represented by floating cylindrical volumes, labeled Andersen "AS" and slit "SS". AS1 and SS1 were located at 1 m, AS2 and SS2 at 2 and 2.5 m, respectively, and AS3 at 1 m to the left of the participant. The subject was approximated by a simplified geometry,[36] having a mouth defined by a circular opening set at a height to match a sitting position. In the experiments, there will have been some variability of the subject's dimensions, along with the distance from the subject's face to the first settle plate.

The chamber was meshed using unstructured tetrahedral cells, with prismatic inflation layers adjacent to the solid surfaces. In the region where the thermal plume from the person impinged on the ceiling, wall y^+ values were approximately 11.5, with an average of 2.5 on the body surface. Mesh refinement was applied in the region of the mouth and the exhaled jet, based on isolated jet simulations. Cell sizes varied from approximately 3 mm at the mouth, to approximately 75 mm in the room, away from walls or openings. The results reported here were obtained on meshes of approximately 655 000 nodes, which provided reasonable run times. A mesh sensitivity study was carried out, which showed that particle sample results were insensitive to further mesh refinement. An explanation for this behavior is that the sampled results are driven by ballistic deposition or sedimentation, rather than wall-parallel flow, where mesh effects can be important. Increasing the overall mesh density to 2.3 million nodes did not appreciably change the diameter ranges or quantity of particles collected by the settle plates or air samplers. The air samplers mainly collected small particles, which are influenced by the room air flow.

3.2 | Boundary conditions

The experiments were carried out at an ambient temperature of 22°C and a relative humidity (RH) of between 44% and 50%. All solid walls were set to the ambient temperature value and the solution initialized with a RH of 50%. As the people in the experiments were fully clothed apart from their face, only the convective heat flux from the subject was modeled, which was applied as a surface heat flux of 25 W/m^2. This value is similar to that measured by Zhu et al.[29] for a resting subject. The inlet of each air sampler was a circular region, set as an outflow through which air was drawn at a constant volume flow rate, equal to the experimental flow rate. The room was specified as being unventilated during the trials, but there was likely to be a small air exchange through the door seal and ventilation system. A pressure boundary matching the position of the ventilation inlet in the chamber was defined (shown in blue in Figure 1B) to balance the outflow of air through the samplers. This was specified as a relative pressure of zero and backflow temperature equal to the room temperature. In practice, the leakage flows are unknown. However, the air velocity through this balancing opening was very small and did not influence the flows in the room.

3.3 | Turbulence modeling

The Reynolds-Averaged Navier-Stokes (RANS) approach was used as it is less computationally intensive than other approaches which aim to directly resolve large-scale turbulent fluctuations. There are numerous RANS turbulence models available which provide good predictions in different types of flows. A challenge is that there is no universally applicable turbulence model which provides optimal predictions in all physical scenarios (e.g., jet flow and near wall flow). Therefore, a level of compromise is often required. Based on initial simulations of buoyancy-driven flow in a room and of an isolated turbulent jet, the k-ω SST model[37] was used across all simulations.

3.4 | Modeling of dispersed respiratory particles

Respiratory particles were modeled using Fluent's multicomponent model. The particles consisted of two components; a solid part (consisting of salts, proteins, and surfactant) specified as non-volatile and a liquid part (water) which could evaporate into the Eulerian phase. All of the solids were grouped into the non-volatile part, with a volume-weighted density calculated from the average of the non-volatile components[1] as shown in Table 1. The resultant average solids density was 1830 kg/m^3, giving the particles initial mass fractions of 98.75% water and 1.25% solids. This water content was similar to the artificial saliva water content described by Walker et al.[20] of 97.9%.

3.4.1 | Momentum exchange

The exchange of momentum between the Eulerian and Lagrangian phases was two-way and accounted for by equating the change of momentum of a particle to the sum of the forces acting on it[38]:

$$\frac{\mathrm{d}p_p}{\mathrm{d}t} = F_D + F_B + F_O \tag{1}$$

The term on the left is the change in particle momentum (kg m/s) and the forces on the right are the drag force (F_D), buoyancy force (F_B), and other forces (F_O), in (N). Virtual mass and pressure gradient forces were not included as the density of the Eulerian phase was

TABLE 1 Particle solids composition, taken from Stettler et al[1]

	Concentration (g/L)	Density (kg/m^3)
Salt	9	2160
Protein	3	1362
Surfactant	0.5	1082

much lower than the particle density.[38] The effects of Brownian motion were not modeled as it has been suggested[39] that the effect is only significant for particles ≤0.03 μm, which is considerably smaller than the particles considered in the current study.

3.4.2 | Turbulent dispersion

Turbulent dispersion introduces a random pattern to the motion of particles, to reflect the effect of small-scale turbulent fluctuations that have been averaged out in the RANS approach. Turbulent dispersion was modeled using the discrete random walk model, DRW,[40] where the drag term in Equation 1 was determined from both the mean flow and a fluctuating component. This fluctuating component was a random proportion of the local RMS value of the velocity fluctuations which were derived from the turbulent kinetic energy of the flow. The default DRW model was implemented so that the same random seed was used for each simulation, such that two simulations run with turbulent dispersion would have identical solutions. The DRW model is known to give poor predictions of wall impaction rates of small particles in wall-parallel flows because of the assumption of isotropic turbulent fluctuations in the two-equation turbulence model RANS approach.[41] However, for this scenario, air flows were low and deposition was likely to be dominated by sedimentation for the majority of the particle sizes. Ceiling and wall deposition rates, where sedimentation does not contribute, were expected to be very small in comparison and were not directly compared in this study.

3.4.3 | Mass transfer

Particle mass transfer was modeled using the diffusion-controlled model,[38] which assumes that the rate of vaporization of component *i* is governed by the concentration gradient between the droplet surface and Eulerian phase:

$$\frac{\mathrm{dm}_i}{\mathrm{dt}} = \mathrm{Sh}\pi \mathrm{d}_p D_i M_{w,i} \left(C_{i,s} - C_{i,\infty}\right) \tag{2}$$

where *Sh* is the Sherwood number (-), which in turn depends on the Reynolds (-) and Schmidt (-) numbers, D_i is the diffusion coefficient (m^2/s), d_p is the particle diameter (m), $M_{w,i}$ is the molecular weight of the component (kg/kmol), and $C_{i,s}$ and $C_{i,\infty}$ are the concentrations (kmol/m^3) at the particle surface and in the Eulerian continuum, respectively.

3.4.4 | Heat transfer

Heat transfer to the particle was modeled using the multicomponent energy equation, accounting for heat transfer by convection and vaporization[38]:

$$m_p C_p \frac{\mathrm{dT}_p}{\mathrm{dt}} = \mathrm{hA}_p \left(T_\infty - T_p\right) + \sum_i h_{fg,i} \frac{\mathrm{dm}_i}{\mathrm{dt}} \tag{3}$$

where m_p is the particle mass (kg), T_p is the particle temperature (K), T_∞ is the continuum temperature (K), C_p is the particle heat capacity (J/kg K), h is the heat transfer coefficient (W/m^2 K), A_p is the particle surface area (m^2), and $h_{fg,i}$ is the latent heat of vaporization of component *i* (J/kg).

3.4.5 | Particle material model

The surface concentration of a solution particle is affected by its composition and the departure from an ideal solution becomes important, especially at high solute fractions. Drying of respiratory droplets has been extensively studied, and there are numerous approaches that can be taken.[18,20] In the current work, the model of Walker et al.[20] was implemented to define the particle surface vapor concentration. For a multicomponent particle, the surface concentration can be given by[38]:

$$C_{i,s} = \gamma_i x_i \varphi_i \frac{P_{\mathrm{sat},i}}{Z^V \mathrm{RT}_p} \tag{4}$$

where γ_i is the activity coefficient (-), χ_i is the component mole fraction (-), φ_i is the fugacity coefficient (-), $P_{\mathrm{sat,i}}$ is the saturation vapor pressure (Pa) at temperature T_p (K), and Z^V is the vapor compressibility (-). For an ideal gas at low pressure, the fugacity coefficient and compressibility are assumed to be equal to 1. Non-ideal solution effects are accounted for through the activity, α_i (-), which is the product of the activity coefficient and component mole fraction[42]:

$$\alpha_i = \gamma_i x_i = \frac{P_i}{P_{\mathrm{sat},i}} \tag{5}$$

where P_i is the modified vapor pressure. Walker et al.[20] parameterized the solute mass fraction, Y_s, (-) in terms of water activity, α_w, for deep lung fluid and artificial saliva. The parameterization for artificial saliva was implemented in Fluent as a lookup table that returned the water activity from the solute mass fraction in the particles. Assuming the solute to be non-volatile, with water being the only vaporizing component, the surface concentration was calculated by

$$C_{w,s} = \alpha_w \frac{P_{\mathrm{sat},w}}{\mathrm{RT}_p}, \alpha_w = f\left(Y_s\right) \tag{6}$$

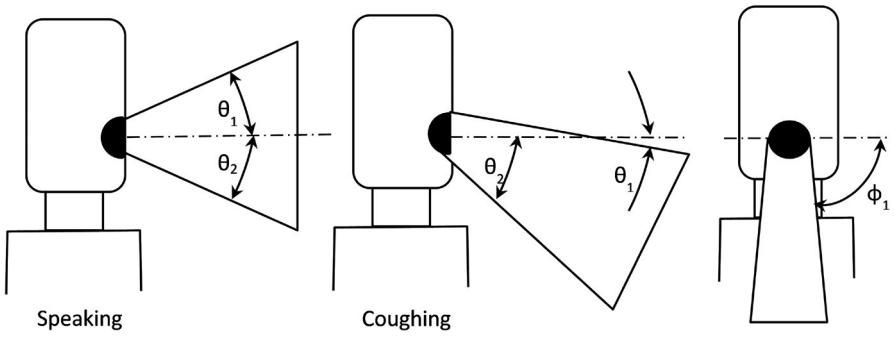

FIGURE 2 Initial jet expansion angles viewed from the side and front. The front projection is the same for both speaking and coughing

To check that the modifications to the material model were correctly implemented, it was compared against data from Hamey[43] using pure water droplets. The model of Walker et al.[20] neglects the effects of surface curvature. The effect was not implemented in the Fluent model as it has been shown to be small for particles greater than 100 nm,[42,44] which represents the majority of particles considered in this study. An additional simplifying assumption was made, based on data in Walker et al.[20], that the models for artificial saliva and deep lung fluid were sufficiently similar that the same material model could be used for all the particles in the simulations.

3.5 | Specification of the exhalation carrier flow

The geometry of the mouth during coughing, talking, and singing is variable and highly uncertain. Rather than attempt to capture these intricacies, exhalations were assumed to originate only from the mouth region which was defined as a circular orifice with a fixed diameter, depending on the activity. A source term was applied over this opening and consisted of a gaseous "carrier" flow with a specified temperature, RH, and transient velocity profile at a particular angle (Figure 2), along with a simultaneous injection of particles. It is known that jet dispersion results are sensitive to the inlet turbulence intensity. There is little available information on this quantity for this specific application, so the intensity and length scale were set as 10% and 0.01 m, respectively.

The details of the modeled carrier flow are given in Table 2. Five different carrier flows were simulated in total. Of the activities listed in the experiments, only the speaking, singing, and coughing activities were modeled. These activities account for the majority of the total exhalation time and have relatively well-defined sources. The carrier flow source terms for talking and singing were implemented as finite duration square waves which did not fully account for the cyclic nature of speech or breathing patterns. To examine the effect of exhalation occurring for only part of the total duration while speaking and singing, modified flows were defined which aimed to capture the maximum velocity projecting the particles, rather than an average. For modified speaking (Source 2), the duration of exhalation was halved and the average flow rate doubled. For modified singing (Source 4), the duration was halved, the average flow rate doubled and then scaled as described in the following section. Coughs are exhalations for their full duration which were approximated as a triangular wave having a duration of 0.4 s and a peak velocity at 0.08 s.[15,16] The carrier flow velocity was spatially varied over the mouth opening within the initial expansion angle, or half cone angle, of the jet, shown in Figure 2. These values were taken from Stettler et al.[1] for speaking and singing and Gupta et al.[15] for coughing. In addition to the humid air flow, an amount of 5% CO_2[45] was included in each carrier flow source term, to explore the dispersion of the carrier flow within the room.

3.6 | Specification of the particle size distribution

The Bronchiolar, Laryngeal, and Oral "BLO" model[13] was used to describe the distribution of exhaled particles. The BLO model describes the particle size distribution for complete exhalations using a tri-modal distribution fitted to experimental measurements of particles from coughing and speaking reported by Johnson and Morawska[46] and Morawska et al.[47].

$$\frac{\mathrm{d\,Cn}}{\mathrm{d\,Log}D} = \ln(10) \times \sum_{i=1}^{3} \left(\frac{\mathrm{Cn}_i}{\sqrt{2\pi}\ln \mathrm{GSD}_i} \right) \exp\left(\frac{\left(\ln D - \ln \mathrm{GMD}_i\right)^2}{2\left(\ln \mathrm{GSD}_i\right)^2} \right) \quad (7)$$

The number concentration, Cn, is the number of particles with diameters in the interval d Log D per cm^3 of exhaled breath, where droplet diameters, D, are measured in μm and d Log D represents a bin width that is constant in base 10 log space. The three modes correspond to sources of exhaled particles within the respiratory system: bronchiolar, laryngeal, and oral. Each mode is fitted with a log-normal distribution. Johnson et al.[13] show parameterization of the distribution with correction factors for dilution and evaporation from measurements made using Aerodynamic Particle Sizers and a spread factor for droplet diameters measured from droplet deposition. The corrected parameters used in these simulations for geometric mean diameter (GMD), geometric standard deviation (GSD), and Cn are shown in Table 3; these are the values suggested by Stettler et al.[1] to describe speaking.

To describe the particles in an exhalation, the droplet diameter range was divided into size bins, allowing the number of particles per cm^3 of exhaled gas and vapor in each size bin to be calculated. The number of particles exhaled for each size bin during an exhalation was the product of the exhalation volume, derived from the

TABLE 2 Specification of the carrier flow using the speaking parameters from Stettler et al[1]

Source and number	(1) Speaking[a]	(2) Modified speaking[b]	(3) Singing[c]	(4) Modified singing[d]	(5) Coughing[e]
Description	Read 1–100	Read 1–100	Happy birthday ×2	Happy birthday ×2	One cough
Diameter (m)	0.015	0.015	0.015	0.015	0.0225
Jet expansion angle θ_1 (deg)	−15	−15	−15	−15	15
Jet expansion angle θ_2 (deg)	15	15	15	15	40
Jet expansion angle φ_1 (deg)	90	90	90	90	90
Temperature (C)	34	34	34	34	34
RH (–)	100	100	100	100	100
Minute vol avg (L/min)	12	24	12	32	180
Duration (s)	50	25	30	15	0.4
Peak time (s)	Steady	Steady	Steady	Steady	0.08
Avg velocity (m/s)	1.11	2.22	1.11	2.99	7.5
Peak velocity (m/s)	1.11	2.22	1.11	2.99	15

[a]Source data taken from Stettler et al.,[1] with an assumed duration.
[b]Source data taken from Stettler et al.,[1] duration halved, flow rate doubled.
[c]The speaking source was used, with an assumed duration.
[d]Modified singing source, based on particle count (see the following section).
[e]Approximated to a triangular waveform from Gupta et al.[15,16]

TABLE 3 Parameters of the BLO model

	Mode 1, bronchiolar	Mode 2, laryngeal	Mode 3, oral
Speaking			
GMD_i (μm)	1.61	2.40	144.7
GSD_i (–)	1.30	1.66	1.80
Cn_i (cm^{-3})	0.0540	0.0684	0.00126
Coughing			
GMD_i (μm)	1.57	1.60	123.3
GSD_i (–)	1.25	1.68	1.84
Cn_i (cm^{-3})	0.0903	0.142	0.0160

parameters in Table 2, and the count density for the size bin. The total number of particles was distributed throughout the duration of each exhalation, and particles were introduced during each of the timesteps used to resolve the exhalation flow. It was assumed that the particle size distribution does not change during exhalations[48] and that the number of particles exhaled varied only with the exhalation flow rate, effectively representing a constant concentration. It was also assumed that the particle velocity vector at the point of injection was equal to the carrier flow velocity at that point. Particles were introduced at random locations over the mouth area and at a random time fraction of each injection time step.

The number of particles emitted during each timestep was calculated as the fraction of the total volume exhaled during the duration of the timestep. Speaking and singing were described by the uniform flow rates given in Table 2, and the exhaled droplets were distributed evenly across the timesteps. For the coughing source having a triangular waveform, the number of particles introduced at each timestep was determined by the fraction of the total volume exhaled during that time interval. At each timestep, the sizes of the particles exhaled were independently sampled from the distribution for the whole of the exhalation. Over the duration of the exhalation, the sampled distribution approached the specified distribution.

The BLO model only gives particle size distributions for speaking and coughing. To reflect the fact that singing will produce a different source characteristic from speaking, a modified singing source (Source 4 in Table 2) was introduced. Gregson et al.[14] presented measurements of speaking and singing made using an Aerodynamic Particle Sizer. This instrument only measured particles up to a diameter of 20 μm, and no corrections were made for the effect of evaporation on the droplet sizes. The measurements presented by Gregson et al.[14] all used the same equipment and experimental approach, allowing comparison of the measurements of speaking and singing. Gregson et al.[14] found that the shape of the droplet distribution was similar to the BLO speaking model of Johnson et al.[13]. For the modified singing source (Source 4), the speaking exhalation flow rate was doubled then scaled by the ratio of the number density of the bronchiolar modes for speaking ($N = 0.74\ cm^{-3}$) and singing ($N = 1.024\ cm^{-3}$) at 90–100 dB.

In a Lagrangian tracking simulation, each computational particle represents a statistical "parcel" of particles. For computational efficiency, a limited number of parcels are usually modeled and each parcel typically represents many individual particles. It is usually advantageous when simulating sprays to track a "statistically significant" number of particles.[49,50] Initial simulations with the BLO model were performed with one particle per parcel (referred to as 1× oversample), so that the count of modeled particles reflected the total count expected for each activity and each simulation effectively represents one realization of each activity. When fitting the BLO model, the full range of exhaled droplet diameters was

broken into 25 equal increments on a base 10 log scale. In some of the increments in the oral mode and between the oral mode and the smaller diameters of the bronchiolar and laryngeal modes, the total number of particles in the increments was small. Sampling from the distribution meant that some increments contained no particles or only one or two particles. To improve the representation of the distribution, simulations were performed using 10 times the number of parcels of particles (referred to as 10× oversample) and the results were scaled accordingly. An additional simulation of one cough was carried out with 100× oversample, but this did not significantly change deposition patterns compared to the 10× oversample simulation. Therefore, 10× oversample counts were used for subsequent simulations. The total parcel counts are shown in Table 4.

3.7 | Simulation strategy

Simulating all the activities sequentially (i.e., coughing, speaking, singing) in a single simulation would result in having to track a large number of particles and would also incur a substantial computational overhead from having to resolve in time each activity in the sequence. For practical purposes, the simulations were carried out individually, where single simulations of one activity (coughing, talking, or singing) were run with subsequent output of particle fates over a 10-min period, corresponding to the experiment, and the particle data were concatenated in post-processing as shown in Table 5. One drawback with this method of simulation is that potential additional dispersive effects of subsequent activities were not accounted for. To further reduce the computing overhead, each 10-min simulation period was divided into three phases: a 30 s initialization phase with a 1 s time step, the activity phase with a finer time resolution of 0.01 s (coughing) or 0.1 s (speaking/singing), and a settling phase lasting the remainder of the duration again having a 1 s time step. These were based on an assessment of the sensitivity of the results to the time step length. In the settling period, the effects of subsequent activities and breathing were ignored.

TABLE 4 Total parcel counts used in the simulations

	Total parcel count		
	1× oversample	10× oversample	100× oversample
One cough	310	3093	30 947
Speaking	1211	12 130	-
Singing	726	7278	-

TABLE 5 Method for concatenating the particle data

Name	Speaking	Singing	Coughing
Standard source	2 × source 1	1 × source 3	6 × source 5
Modified source	2 × source 2	1 × source 4	6 × source 5

4 | RESULTS

The experimental data were presented as the mean number of bacterial colony-forming units (CFUs) recovered from each sample plate and aerosol sampler, with error bars to represent one standard deviation. This was considered an appropriate measure for comparison against computational results. It should be noted that the generation of bacteria was variable by person; one participant generated 39% of all deposited bacteria and 29% of airborne particles, and 50% of participants generated 80% of deposited and airborne bacteria.

In comparing the computational results to experimental data, it was assumed that the collection efficiency of the aerosol samplers was 100% for all sizes. Sample results were compared with the predicted concatenated cumulative particle dataset, where for the idealized case it is assumed that each sampled computational particle results in a bacterial colony and the number of sampled computational particles can be directly compared to the experimental data. For the k^{th} sample location, the total number of particles, N_k, can be defined as follows:

$$N_k = N_{\text{parcels},k} \times N_p \tag{8}$$

where $N_{\text{parcels},k}$ is the number of sampled parcels and N_p is the number of particles per parcel. An alternative measure is to compute relative counts which can be used to assess the level of dispersion among the sample locations. The first centerline settle plate (PCL1) was chosen to normalize the results, to give a normalized count, $N_{\text{norm},k}$, as follows:

$$N_{\text{norm},k} = \frac{N_{\text{parcels},k}}{N_{\text{parcels,PCL1}}} \tag{9}$$

Results from the experiment were normalized in the same way, using the count on the first settle plate. The viability of airborne bioaerosols is influenced by a number of factors[51] so the count of modeled particles may tend to overestimate the number of viable particles emitted. In this case, viable refers to the initial probability of a particle containing viable material, it does not account for further effects such as culturability, damage due to drying, or the possibility that the final dried particle diameter might be smaller than the dimension of a bacteria. The mean number of colony-forming units in a particle of initial diameter, d_0, can be expressed by[52]:

$$\mu = \frac{\pi}{6} d_0^3 C_b \tag{10}$$

where C_b is the mean number of aerobic bacteria cultured and was estimated from the experiments to be 7.37×10^7 CFU/ml (SD: $\pm 6.43 \times 10^7$, range 1.5×10^7 CFU/ml to 2.37×10^8 CFU/ml). Assuming a Poisson distribution, the probability that a particle will contain at least one CFU is given by[52]:

$$P = 1 - e^{-\mu} \tag{11}$$

Figure 3 is a plot showing the variation of P with particle diameter for the range of C_b given above. The number of viable particles, $N_{viable,k}$, at the k^{th} sample location was calculated by:

$$N_{viable,k} = N_p \sum_k P \tag{12}$$

4.1 | Overall comparisons in air and on surfaces

Comparisons between the measured experimental microbial data and simulated particle counts in air and on surfaces are shown in Figure 4. Both experimental and computational results show the same trends, with greater deposition onto surfaces closer to the source than at a further distance. Experimental results also clearly show that exhaled bacteria are present in the air and on surfaces at 2 m from the source. The number of bacteria that deposit at 2 m is around a quarter of the number at 0.2 m, but the particle count extracted from the air in this small unventilated chamber is actually greater at 2 m than at 1 m, and greater than that deposited onto surfaces.

Results for the centerline settle plates are shown in Figure 4A, using the idealized particle count given by Equation 8. Particle count on the closer plates is overpredicted with those on the first plate overpredicted by a factor of five. One reason for this overprediction is that every particle that lands on a plate is counted in the simulation, whereas in the experiment, only those that form a culture can be recorded. The modified source terms for speaking and singing resulted in slightly increased deposition on the nearest plates, due to the increased particle input velocity. However, most of the particles deposited on the plates were from the coughing activity and the contribution of speaking and singing to the total count on the plates remained small. Figure 4B shows a comparison of the viable particles for the centerline plates, using Equation 12. The results are the same as the idealized case for the first two plates where the rapid deposition of larger particles dominate. Further away, the predicted viable count decreases compared to the idealized case. The results with the normalized particle count using Equation 9 shown in Figure 3C show that the simulated rate of decay with distance is steeper than seen in the experiments with a greater number of bacteria collected on the more distant plates than predicted. This is likely to be a result of the variability within the experiments, including individual differences in exhalation velocities and particle size ranges which was not fully replicated in the simulation. The simulated input carrier flow was fixed in each case such that variability was only included in the particle oversampling, which only accounts for part of the overall variability. The order of magnitude difference in counts on the plates observed between individuals is not represented in the model. In the model, no particles were predicted on the off-axis plates to the right of the subject and so are not shown in the figures. A small number of particles were collected on these plates in the experiment.

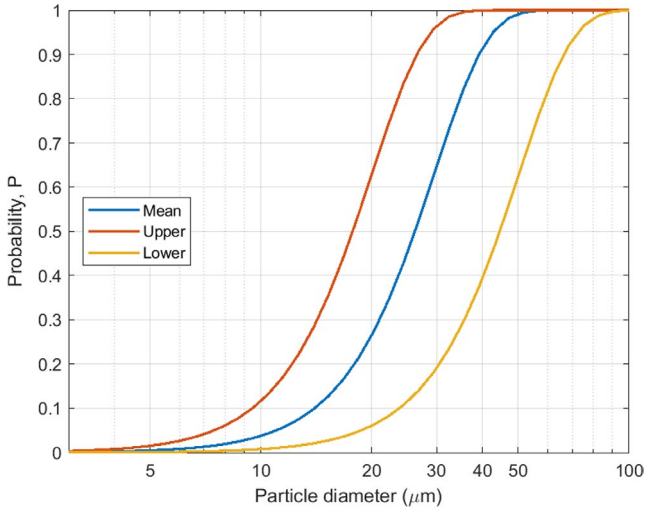

FIGURE 3 Variation of the probability, P, that a particle will contain at least one CFU with particle diameter

Results for the Andersen air samplers are shown in Figure 4D-F. The model overpredicted absolute counts at the inline samplers (AS1, AS2), see Figure 4D, while no particles were predicted to be collected by the off-axis sampler to the left of the person (AS3) although samples were collected in the experiments. Figure 4E shows the adjusted results for the Andersen air samplers, accounting for the viability of the particles are significantly different. In the model, these samplers collected only the smallest particles (<10 μm), which have a lower probability of containing viable bacteria. It is likely that these results are heavily influenced by the initial particle size distribution. Figure 4F shows that relative collection was around three times higher at the 1 m sampler in the simulation, whereas at 2 m the experimental and computational results are similar. Further analysis of the model results showed that a chamber length recirculation, driven by the subject's thermal plume, was transporting particles from the ceiling toward the end of the room and down the end wall (Figure 5). This may explain why the second Andersen sampler (AS2) in the experiment collected a relatively large number of particles.

In the model, this recirculation also resulted in an increased predicted particle count in the slit sampler adjacent to the end wall. The air sampler results suggest that the dispersion off the centerline axis is being underpredicted. There are several reasons why this may have occurred. Firstly, it is likely that there were small but finite ventilation flows in the experimental chamber that were not captured by the model, such as leaks through the door or ventilation panels, air movements due to the movement of the subjects, residual air movements from setting up the experiments or residual air movements from ventilation. Secondly, in the experiments, each activity was carried out in succession and this would have had a mixing effect on the particles exhaled from the previous activities. This effect would not have been captured in the simulations, where each activity was carried out in isolation. Finally, the intra-person variability would have resulted in a wider spread of data, while parameters such as the carrier flow and projection angles were fixed in the simulations.

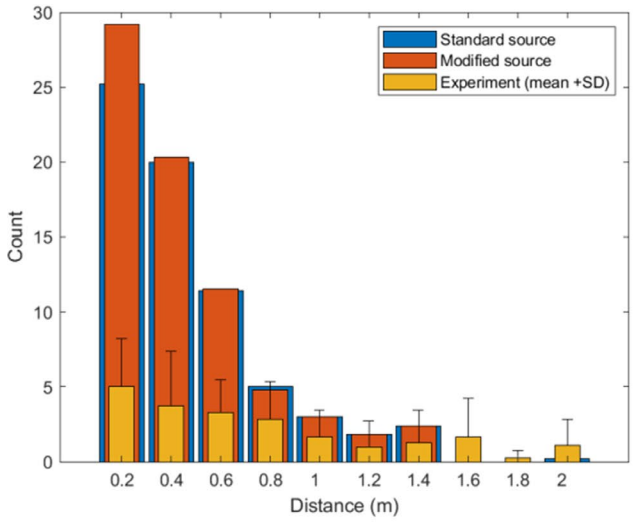

(A) Cumulative results, centreline (count)

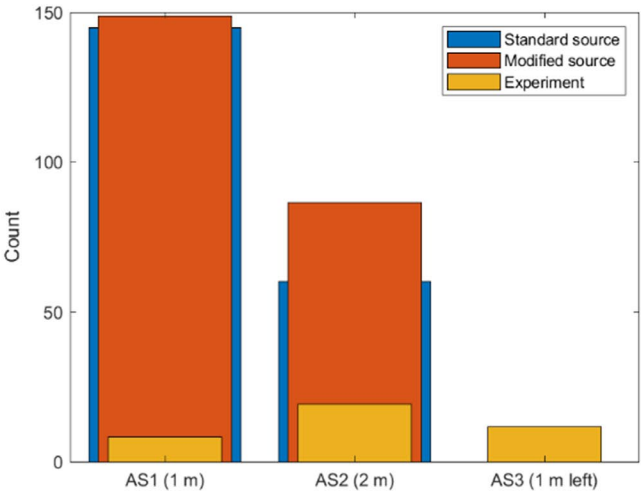

(D) Cumulative results, Andersen (count)

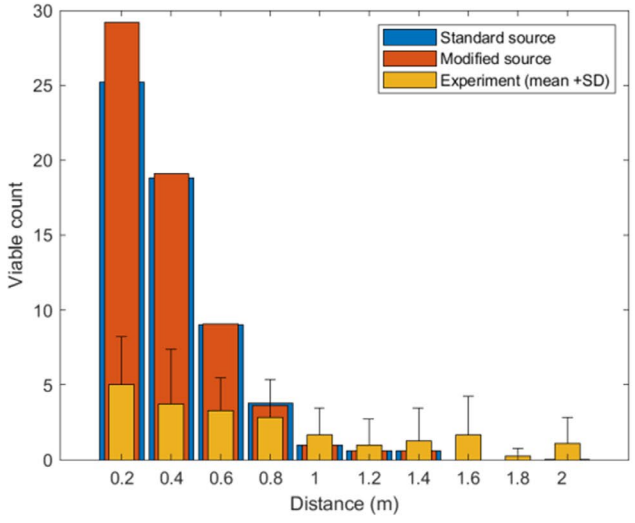

(B) Cumulative results, centreline (viable count)

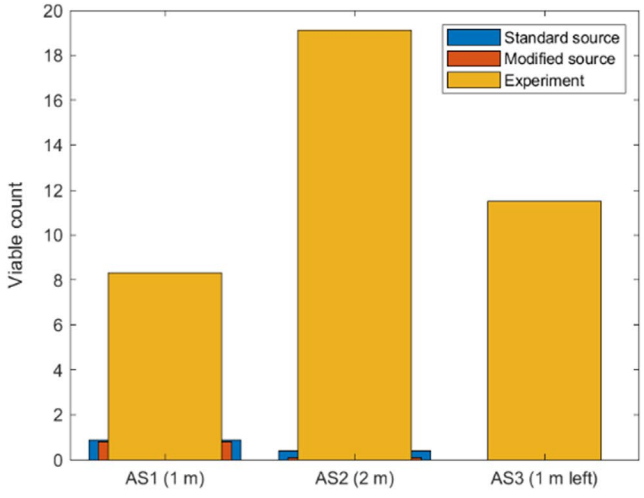

(E) Cumulative results, Andersen (viable count)

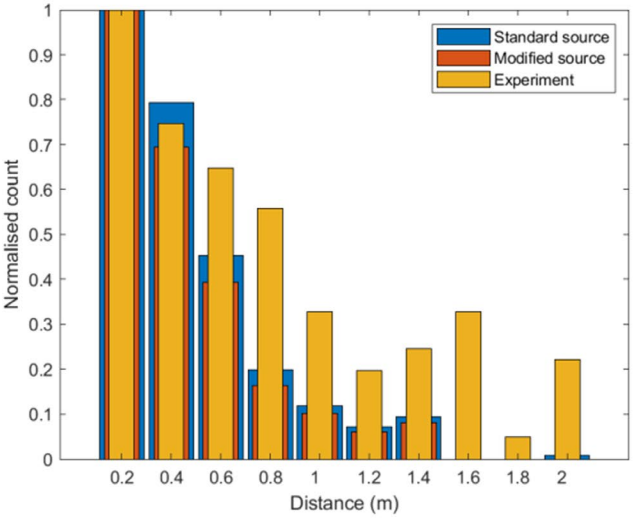

(C) Cumulative results, centreline (normalised count)

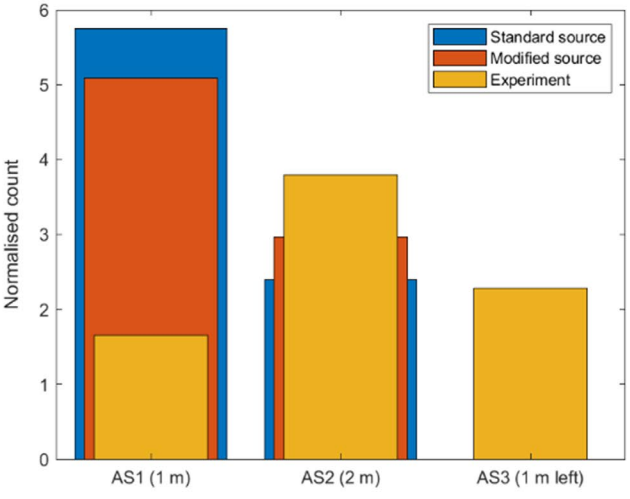

(F) Cumulative results, Andersen (normalised count)

FIGURE 4 Comparison of measured (mean + SD) microbial counts (yellow) with simulated predicted counts at the sample locations using different metrics and the standard source (blue) and modified source (orange). Cumulative counts were obtained from the concatenated datasets for each activity at each location. (A and D) show actual simulated number of particles, (Equation 8). (B and E) show predicted number of viable particles, (Equation 12), (C and F) show normalized count (Equation 9)

FIGURE 5 Contour plots of velocity magnitude, in m/s, and particle locations, at two time intervals after the end of speaking. The contours are clipped to a maximum of 0.2 m/s to highlight the recirculation flow induced by the thermal plume

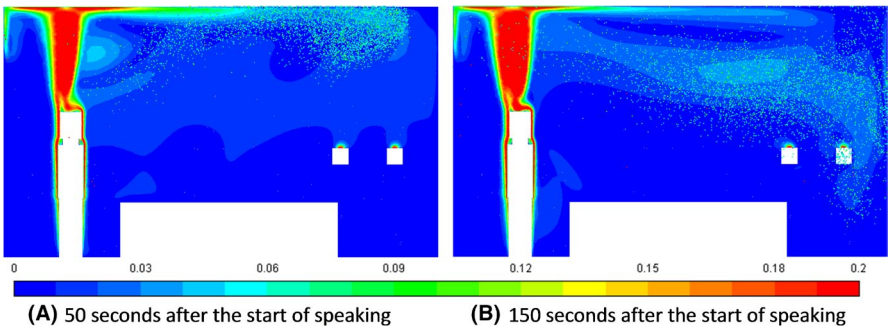

4.2 | Analysis of particle sizes

Figure 6 shows the partitioning of sampled particle sizes from the CFD simulations on the surfaces and collected in the air samples, for each individual activity. In each case, the count refers to the number of parcels sampled at each location and these are compared with the input number of parcels shown in blue. The diameters in Figure 6 are the initial diameters of the particles at their time of injection, for both input and sampled particles; although the diameter change due to evaporation is modeled, the comparison is made using the initial diameters to illustrate the ultimate fate of different sizes of exhaled particles. For clarity, the surface samples were grouped together into "Centreline plates" (orange), "Centreline tables" (purple), "Right table" (green), and "Floor" (light blue). The right hand plates are not included in these plots, because no particles were predicted to deposit there. The air samples are recorded at "AS1" (orange), "AS2" (yellow), "SS1" (purple), and "SS2" (green), see Figure 1B. The general trend is that the larger particles, representing the oral mode of production, were deposited on surfaces. The predicted air samples were generated entirely by the bronchiolar and laryngeal modes from the input BLO particle distribution. The exception was the cough, in which most of the full range of sizes was projected on to the surfaces. This partitioning of diameters between surfaces and air samples appears to be, in part, due to the droplet diameter distribution in the BLO model which has a pronounced dip in the initial diameter distribution, around 30 μm, between B and L, and O modes.

4.3 | Influence of evaporation

Figure 7 shows the change in particle diameters from the original to the diameter at the point of sampling for the three activities. Sampled particles are those collected on a surface, extracted by the air samplers or those remaining suspended at the end of the simulation period. The results suggest that the division between the B/L and O modes remains pronounced at the point that particles are sampled. Small particles have relatively fast evaporation timescales but longer persistence in the air. Larger particles have slower evaporation timescales but are sampled relatively quickly on surfaces.

Figure 8 shows, for the model, the ratio of the number of sampled particles of each diameter to that at the source for each of the air samplers. The horizontal lines represent the analogous ratio of the total volume of CO_2 extracted at a sample point to the total volume of CO_2 introduced at the mouth. The off-axis air sampler (AS3) to the left of the subject is not included in these plots as no particles were predicted at that location. It is clear, for the number of particles simulated, that the CO_2 is more diffusive than the particles. This can be seen as, overall, the ratio of sampled to input CO_2 is lower than for the particles. Some CO_2 reached the off-axis air sampler (AS3) to the left of the subject for speaking and singing, though this was a small amount and only occurred in the final stages of the simulations. The proportioning of CO_2 and particles among the samplers shows similar patterns, that is, more particles and CO_2 were recorded in samplers close to the source (AS1, SS1) for coughing, while more were registered at the furthest sampler (SS2) for speaking and singing.

5 | DISCUSSION

The CFD-based exhalation model developed in this study takes into account exhalation flows, particle size distributions, evaporation effects, and the fraction of microbial material contained within respiratory particles. The model follows the Euler-Lagrange framework of previous CFD studies and therefore would be expected to perform in a similar way to those models. Validation of complete exhalation models of this type is challenging due to the lack of suitable experimental data and reliance is placed on validation of individual components of a model (exhalation jet, indoor air flows). Comparisons with a human participant study showed that the model is able to produce realistic predictions of microbial surface deposition and

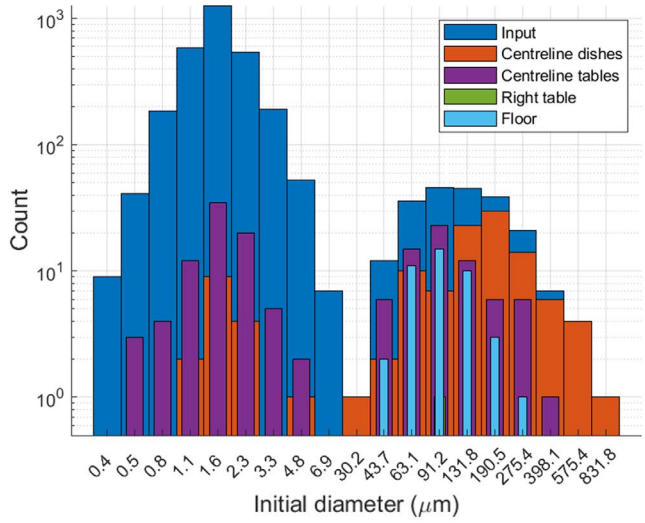

(A) surface sample count, one cough

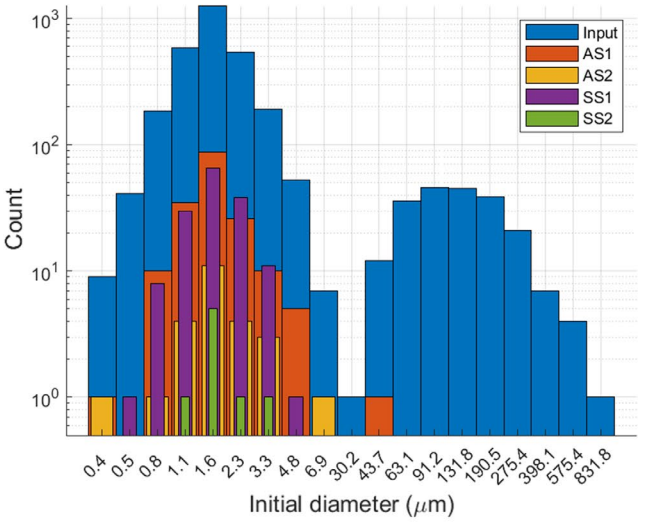

(D) air sample count, one cough

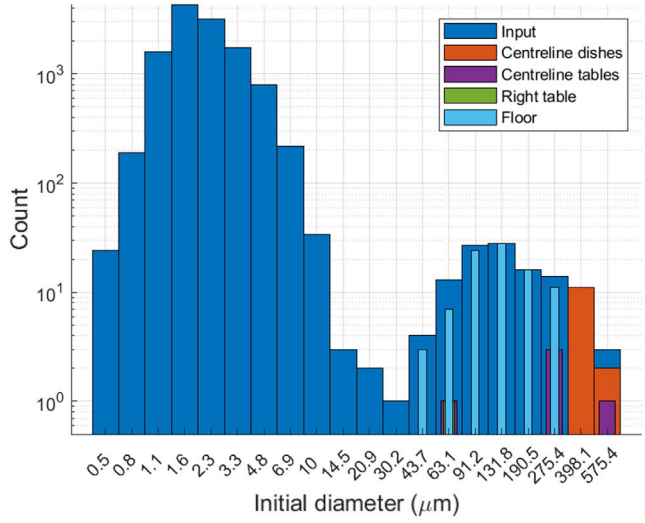

(B) surface sample count, speaking

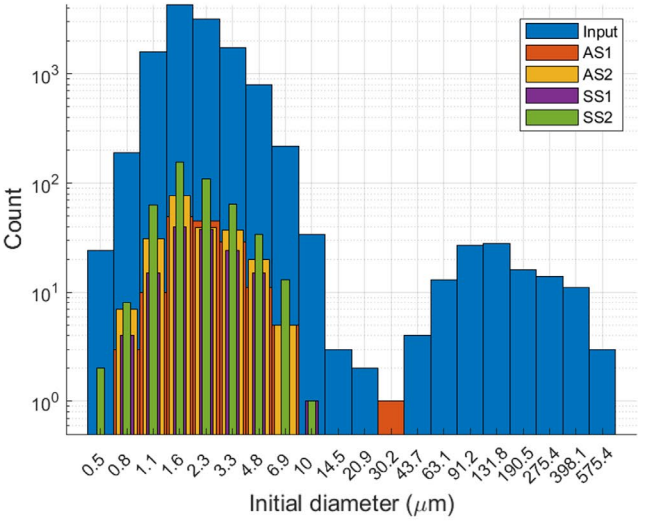

(E) air sample count, speaking

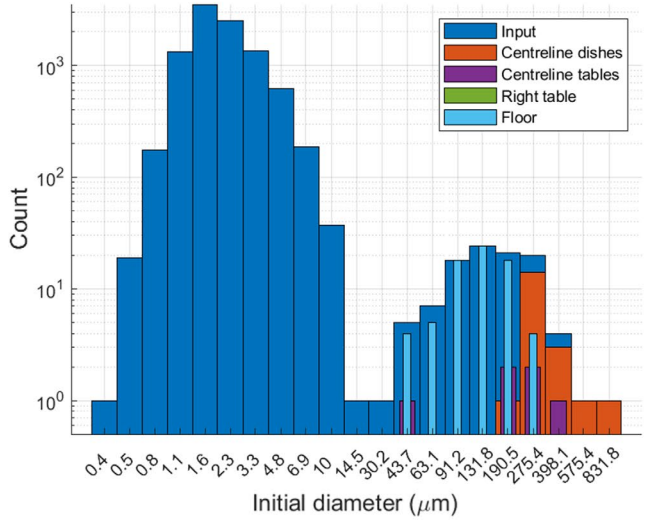

(C) surface sample count, singing

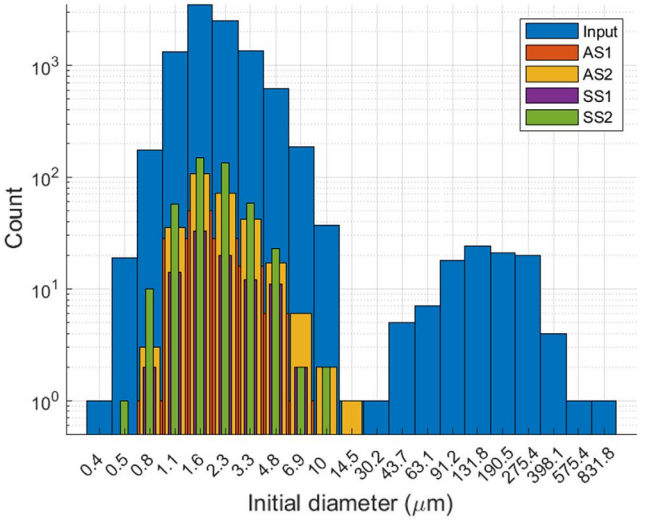

(F) air sample count, singing

FIGURE 6 Comparison of sampled particle diameters with the input diameters. On the left (A-C) are all of the surface samples for coughing, talking, and singing, respectively, and on the right (D-F) are the corresponding air samples. In each case, the diameter is the initial diameter of the particles at their time of injection, irrespective of their diameter at the point of sampling

concentrations in air, although it may slightly underpredict the distance traveled by both aerosols and droplets. Given the uncertainties involved in simulating these experiments, the computational

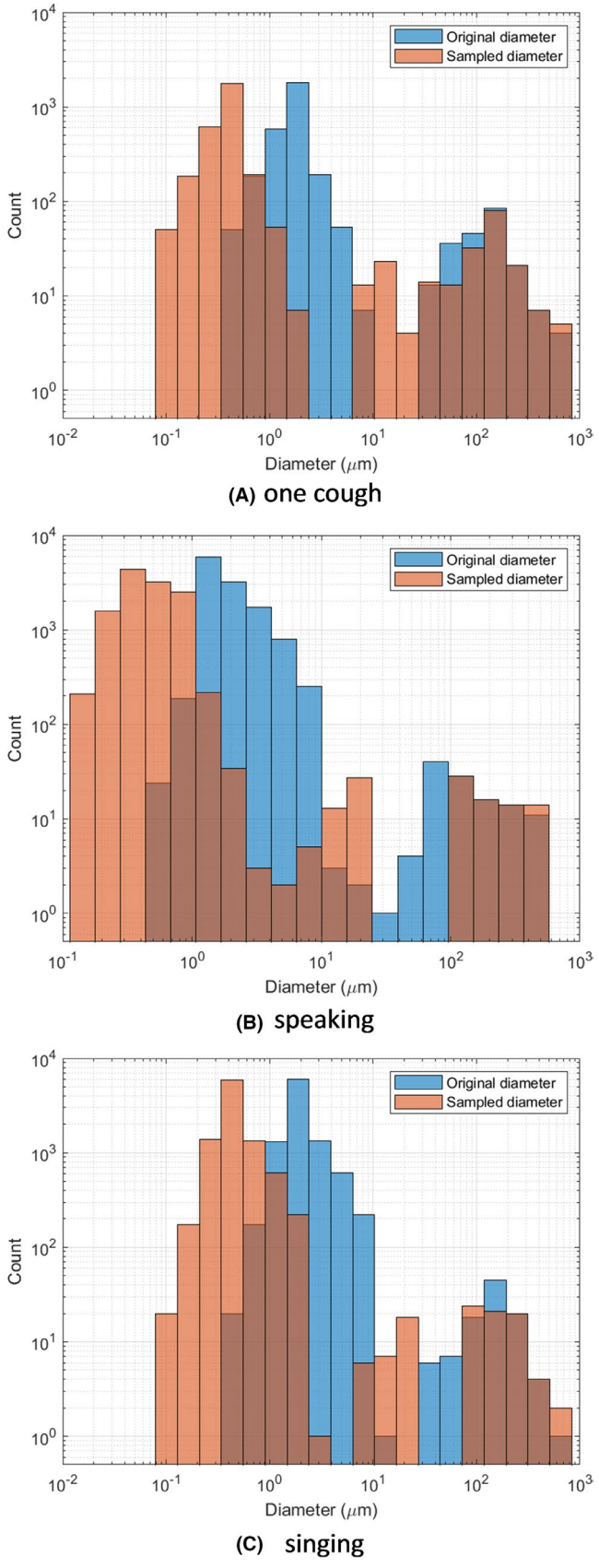

FIGURE 7 Comparison of model particle counts for the initial (blue) and sampled (orange) diameters. In addition to deposited and extracted particles, any suspended particles at the end of the simulations were counted as sampled. The darker shaded bars are where both input and samples overlap

results obtained on the centerline were particularly encouraging. The discrepancies seen off-axis require further investigation to understand the variability in the experimental study deposition results. The simulations are based on a mostly uniform set of conditions and therefore will not capture much of the intra- and inter-person variability seen in the volunteer experiments. In a modeling study, the effects of this variability can be further understood through a sensitivity analysis of the type reported by Ho.[26] However, this would be a significant computational undertaking without making numerous simplifying assumptions.

The approach taken in the current modeling study was to implement a practicable estimate for a source term for different exhalation activities, and to simulate activities separately and sum the effects rather than simulate sequentially. Some variability has been included through the use of 10-time oversampled particles, giving a greater spread of particle injection times and velocities. However, the off-axis samples are likely to be influenced by aspects of the ventilation flow that were not accounted for in the simulations where it was assumed that the flow of air drawn by the samplers was balanced by that through a single vent panel. In practice, there will have been small but finite air flows through the doors and other ventilation controls which may have increased mixing within the chamber. In addition, the thermal conditions in the experiment may differ from the idealized case simulated and the sequence of vocal activities in the experiment would contribute to the overall mixing in the room.

The model results depend on a number of assumptions and input models, including the need to specify emission rates of respiratory droplets and aerosols and exhalation parameters such as velocity and angle of the jet. The use of the BLO model[13] resulted in a fairly clear distinction between particles that would remain airborne and those which deposit relatively quickly,however, it is noted that the bimodal distribution is not seen in other measured data[12] and may be related to how the different size categories of respiratory particles are measured and sampled. The BLO model is based on data collected over multiple studies, with multiple volunteers and using different measuring techniques. It is representative across the range of measured particle sizes. However, it is recognized that there is an inherent variability in such measurements and that other particle size distributions could be used. The model also assumed that microorganisms were uniformly distributed by volume, which may not be the case if there is preferential aerosolization into smaller or larger sizes due to hydrophobicity effects, or clumping of bacteria.

Despite these uncertainties, the model results showed similar behavior to the experiments in that deposition was greater at 1 m than at 1–2 m from source and the results from the air samplers suggested that fine (approx. 0.4–10 μm) particles would eventually be uniformly suspended in the room given sufficient mixing time.

This suggests that a computational model based on parameters from measured aerosol and exhalation data and the physics of droplet evaporation can provide realistic representations of the fate of exhaled microbial particles.

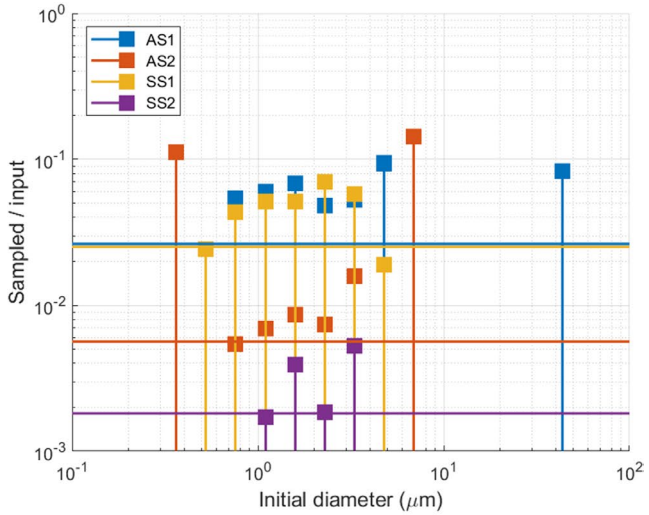

(A) CO_2 ratio, one cough

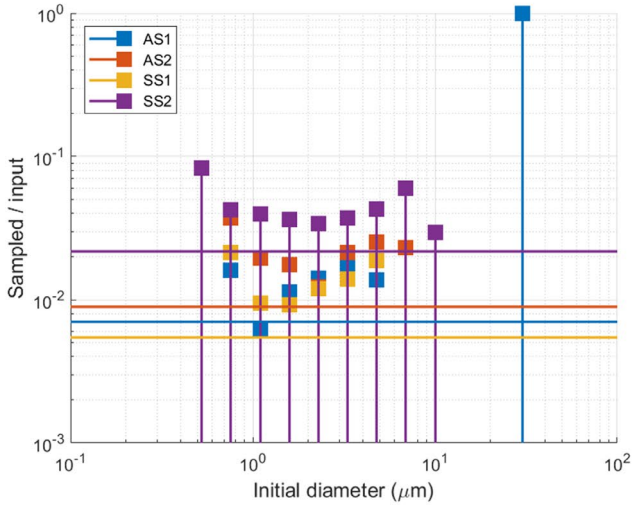

(B) CO_2 ratio, speaking

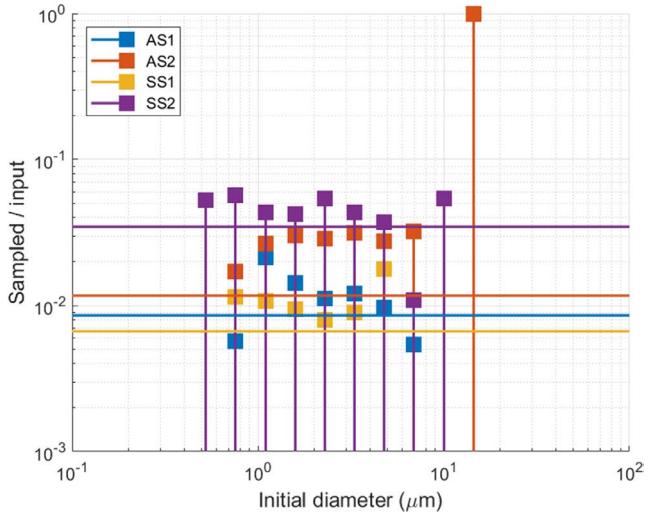

(C) CO_2 ratio, singing

FIGURE 8 Ratio of the modeled number of air sampled particles to the input number of particles, by diameter, for (A) a cough, (B) talking, and (C) singing. The horizontal lines represent the ratio of sampled to input CO_2 concentration. The CO_2 ratios at AS1 and SS1 for one cough are overlaid

5.1 | Implications for SARS-CoV-2 virus transmission

The model presented here is compared to oral and respiratory bacteria rather than the SARS-CoV-2 virus, as it was not feasible to carry out experiments with COVID-19 patients. Although bacteria are larger than viruses (typically 1–2 μm in diameter compared to around 0.07–0.09 μm), respiratory aerosols carrying virus will also carry the same salts, surfactants, and proteins in our study and will also carry oral and respiratory tract bacteria. Viral aerosols may be able to evaporate to smaller sizes, but many will still be likely to be a similar size to those measured in this study. Estimates of SARS-CoV-2 viral load in respiratory fluid span many orders of magnitude, and the value depends on a number of factors including the source of the respiratory fluid, the stage of the disease, and the sampling method used to collect the data. Stettler et al.[1] report values ranging from an average of 1.18×10^6 copies/ml of sputum to as high as 1.34×10^{11} copies/ml based on data from nasopharyngeal and throat swabs, while Chen et al.[53] report from a meta-analysis of 64 studies that the 90th percentile viral load was $1 \times 10^{9.84}$ copies/ml. Information on the decay of virus in exhaled droplets is also sparse.[54] However, the values provided may enable initial estimates of the range of viral exposure that may be expected in both deposited droplets and aerosols. The current model has shown that surface deposition and air concentration reduce with distance and confirms guidance that indicates that there is likely to be a reduced direct inhalation exposure or fomite risk to someone over 2 m away face-to-face with the source. However, it is recognized that fomite risk remains after a person has moved allowing others to be potentially exposed. The model also highlights the potential for greater exposure in a poorly ventilated space, with no clear relationship between particles that remain airborne and distance in the results presented here. The current study aimed to develop and validate a methodology that can be used for more extensive airborne transmission studies such as exploring the influence of measures such as room internal layout, social distancing, physical screens and barriers and ventilation strategies. The model outputs may also provide data on inhalation exposure with distance and surface contamination for faster running infection risk models such as those used to model transmission in healthcare[55] and on a cruise ship.[56] Further work is needed to quantify virus decay in deposited or airborne droplets and to consider dose–response in a susceptible individual.

6 | CONCLUSIONS

A CFD model of exhalations has been developed and compared with experimental data for the dispersion of bacteria from subjects

coughing, speaking, and singing in a room. On the basis of normalized particle count, to assess the relative dispersion among the sample locations, the model performed reasonably well, particularly given the uncertainties involved at all stages of the modeling. There was also relatively good agreement in the ratio of particle counts among the surface samples and air samples in front of the subject, although deposition on sample plates close to the participants and the rate of reduction of particle count with distance were both overpredicted. Off-axis dispersion was relatively poorly predicted, suggesting that the dispersion in the test chamber as a whole was being underpredicted, probably due to air movement during the experiments that were not accounted for in the model. The model appeared to capture a flow recirculation that carried particles along the upper part of the chamber and down toward the air samplers. This effect was more pronounced in the air sampler adjacent to the end wall (SS2) than the one at the end of the tables (AS2).

Comparison of absolute bacterial colony counts showed that the model performed relatively well, given the variability in initial bacterial load and uncertainty in particle size distributions. When the bacterial load in the particles was simulated by applying a Poisson distribution based on the initial particle diameter, the results became skewed toward deposition on the sample plates. An explanation for this is the relatively small diameter airborne particles predicted by the BLO model. The model results showed a distinct partitioning between 0.4–10 μm particles which remained airborne and 30–600 μm particles which deposited on surfaces, especially in the case of speaking and singing. This effect was less pronounced in coughing, which tended to direct particles of all diameters onto the surfaces.

Both the model and experiments showed similar trends and clearly demonstrated that exhaled microorganisms can travel 2 m and remain suspended in the air within a room. The model results showed similar behavior to the experiments in that significant deposition was recorded at around 1 m from the source but then dropped off quickly over the next meter. The results from the air samplers suggested that fine particles would eventually be uniformly suspended in the test chamber given sufficient mixing time. Comparison of predicted and experimental results was encouraging and has provided confidence that the computational methodology can be used for more extensive airborne transmission studies. In particular, an aim for future work would be to determine how different source terms translate into viral loadings in the environment.

ACKNOWLEDGEMENTS

The authors would like to acknowledge funding provided through PROTECT, the National Core Study on Transmission and the Environment which partially funded this work. The contents of this paper, including any opinions and/or conclusions expressed, are those of the authors alone and do not necessarily reflect HSE policy.

CONFLICT OF INTEREST

No conflict of interest declared.

AUTHOR CONTRIBUTIONS

SimonColdrick: Methodology (equal); software (lead); writing – original draft preparation(lead). Adrian Kelsey: Formal analysis (lead); methodology (equal); writing – originaldraft preparation (supporting). Matthew Ivings: Methodology (equal); supervision(lead); writing – review & editing (supporting). Timothy Foat: Methodology(equal); writing – review & editing (supporting); software (supporting). SimonParker: Methodology (equal); conceptualization (supporting); writing – originaldraft preparation (supporting). Catherine Noakes: Conceptualization (lead); writing–original draft preparation (supporting). Allan Bennett: Investigation (lead);writing – original draft preparation (supporting). Helen Rickard: Investigation(supporting); writing – original draft preparation (supporting). Ginny Moore: Investigation(supporting); writing – original draft preparation (supporting).

REFERENCES

1. Stettler M, Nishida RT, de Oliveira PM, et al. Source terms for benchmarking models of SARS-CoV-2 transmission via aerosols and droplets, submitted to Royal Society Open Science, 2021.
2. Xie X, Li Y, Chwang ATY, Ho PL, Seto WH. How far droplets can move in indoor environments-revisiting the Wells evaporation-falling curve. *Indoor Air*. 2007;17(3):211-225.
3. Nicas M, Nazaroff WW, Hubbard A. Toward understanding the risk of secondary airborne infection: emission of respirable pathogens. *J Occup Environ Hyg*. 2005;2(3):143-154. doi:10.1080/15459620590918466
4. Coleman KK, Tay DJW, Tan KS, et al. Viral load of severe acute respiratory syndrome Coronavirus 2 (SARS-CoV-2) in respiratory aerosols emitted by patients with coronavirus disease 2019 (COVID-19) while breathing, talking, and singing. *Clin Infect Dis*. 2021:ciab691, 10.1093/cid/ciab691
5. Lindsley WG, Blachere FM, Thewlis RE, et al. Measurements of airborne influenza virus in aerosol particles from human coughs. *PLoS One*. 2010;5(11):e15100. doi:10.1371/journal.pone.0015100
6. Gordon MH. House of Commons (Ventilation). Report and recommendations, December 1904; 1905. (HC 1905 Cd. 2404).
7. Riley RL. Airborne pulmonary tuberculosis. *Bacteriol Rev*. 1961;25(3):243-248.
8. Remington PL, Hall WN, Davis IH, Herald A, Gunn RA. Airborne transmission of measles in a physician's office. *JAMA*. 1985;253(11):1574-1577.
9. Tellier R. Review of aerosol transmission of influenza A virus. *Emerg Infect Dis*. 2006;12(11):1657-1662. doi:10.3201/eid1211.060426
10. Li Y, Huang X, Yu ITS, Wong TW, Qian H. Role of air distribution in SARS transmission during the largest nosocomial outbreak in Hong Kong. *Indoor Air*. 2005;15(2):83-95. doi:10.1111/j.1600-0668.2004.00317
11. World Health Organisation Transmission of SARS-CoV-2: implications for infection prevention precautions: scientific brief, 09 July 2020. World Health Organization. https://apps.who.int/iris/handle/10665/333114 Accessed March 1, 2021
12. Duguid JP. The size and the duration of air-carriage of respiratory droplets and droplet-nuclei. *Epidemiol Infect*. 1946;44(6):471-479.
13. Johnson GR, Morawska L, Ristovski ZD, et al. Modality of human expired aerosol size distributions. *J Aerosol Sci*. 2011;42:839-851.
14. Gregson FKA, Watson NA, Orton CM, et al. Comparing the respirable aerosol concentrations and particle size distributions generated by singing, speaking and breathing. *ChemRxiv*. 2020. 10.26434/chemrxiv.12789221.v1
15. Gupta JK, Lin CH, Chen Q. Flow dynamics and characterization of a cough. *Indoor Air*. 2009;19(6):517-525.

16. Gupta JK, Lin CH, Chen Q. Characterizing exhaled airflow from breathing and talking. *Indoor Air*. 2010;20(1):31-39.
17. Chen W, Zhang N, Wei J, Yen HL, Li Y. Short-range airborne route dominates exposure of respiratory infection during close contact. *Build Environ*. 2020;176:106859.
18. de Oliveira PM, Mesquita LC, Gkantonas S, Giusti A, Mastorakos E. Evolution of spray and aerosol from respiratory releases: theoretical estimates for insight on viral transmission. *Proc Roy Soc A Math Phys Eng Sci*. 2021;477(2245):20200584
19. Wei J, Li Y. Enhanced spread of expiratory droplets by turbulence in a cough jet. *Build Environ*. 2015;93:86-96.
20. Walker JS, Archer J, Gregson FK, Michel SE, Bzdek BR, Reid JP. Accurate representations of the microphysical processes occurring during the transport of exhaled aerosols and droplets. *ACS Cent Sci*. 2021;7(1):200-209.
21. Noakes CJ, Sleigh PA. Mathematical models for assessing the role of airflow on the risk of airborne infection in hospital wards. *J R Soc Interface*. 2009;6:S791-S800.
22. Burridge HC, Fan S, Jones RL, Noakes CJ, Linden PF. Predictive and retrospective modelling of airborne infection risk using monitored carbon dioxide. *Indoor Built Environ*. 2021;1–18. doi:10.1177/1420326x211043564
23. Jones B, Sharpe P, Iddon C, Hathway EA, Noakes CJ, Fitzgerald S. Modelling uncertainty in the relative risk of exposure to the SARS-CoV-2 virus by airborne aerosol transmission in well mixed indoor air. *Build Environ*. 2021;191:107617.
24. Chen C, Zhao B. Some questions on dispersion of human exhaled droplets in ventilation room: answers from numerical investigation. *Indoor Air*. 2010;20(2):95-111.
25. Feng Y, Marchal T, Sperry T, Yi H. Influence of wind and relative humidity on the social distancing effectiveness to prevent COVID-19 airborne transmission: a numerical study. *J Aerosol Sci*. 2020;147:105585.
26. Ho CK. Modeling airborne pathogen transport and transmission risks of SARS-CoV-2. *Appl Math Model*. 2021;95:297-319.
27. Li H, Leong FY, Xu G, Ge Z, Kang CW, Lim KH. Dispersion of evaporating cough droplets in tropical outdoor environment. *Phys Fluids*. 2020;32(11):113301.
28. Redrow J, Mao S, Celik I, Posada JA, Feng ZG. Modeling the evaporation and dispersion of airborne sputum droplets expelled from a human cough. *Build Environ*. 2011;46(10):2042-2051.
29. Zhu S, Kato S, Yang JH. Study on transport characteristics of saliva droplets produced by coughing in a calm indoor environment. *Build Environ*. 2006;41(12):1691-1702.
30. Villafruela JM, Olmedo I, Ruiz de Adana M, Méndez C, Nielsen PV. CFD analysis of the human exhalation flow using different boundary conditions and ventilation strategies. *Build Environ*. 2013;62:191-200.
31. King M-F, Noakes CJ, Sleigh PA, Camargo-Valero MA. Bioaerosol deposition in single and two-bed hospital rooms: a numerical and experimental study. *Build Environ*. 2013;59:436-447.
32. Dada AC, Gyawali P. Quantitative microbial risk assessment (QMRA) of occupational exposure to SARS-CoV-2 in wastewater treatment plants. *Sci Total Environ*. 2021;763:142989. doi:10.1016/j.scitotenv.2020.142989
33. Chen F, Simon CM, Lai AC. Modeling particle distribution and deposition in indoor environments with a new drift–flux model. *Atmos Environ*. 2006;40(2):357-367.
34. Parker S, Nally J, Foat T, Preston S. Refinement and testing of the drift-flux model for indoor aerosol dispersion and deposition modelling. *J Aerosol Sci*. 2010;41(10):921-934.
35. ANSYS. *Fluent, Release 19.0, User's Guide*. ANSYS Inc; 2019.
36. NASA Man-Systems Integration Standards Revision B, Volume I, Section 3 Anthropometry and Biomechanics; 1995. https://msis.jsc.nasa.gov/sections/section03.htm Accessed March 1, 2021
37. Mentor F. Two-equation eddy-viscosity turbulence models for engineering applications. *AIAA J*. 1994;32:1598-1605.
38. ANSYS. *Fluent, Release 19.0, Theory Guide*. ANSYS Inc; 2019.
39. Ounis H, Ahmadi G, McLaughlin JB. Brownian diffusion of submicrometer particles in the viscous sublayer. *J Colloid Interface Sci*. 1991;143(1):266-277.
40. Gosman AD, Ioannides E. Aspects of computer simulation of liquid-fuelled combustors. *J Energy*. 1983;7(6):482-490.
41. Parker S, Foat T, Preston S. Towards quantitative prediction of aerosol deposition from turbulent flows. *J Aerosol Sci*. 2008;39(2):99-112.
42. Seinfeld JH, Pandis SN. *Atmospheric Chemistry and Physics: From Air Pollution to Climate Change*. John Wiley & Sons; 2016.
43. Hamey PY. The evaporation of airborne droplets, MSc Thesis. Cranfield University, Bedfordshire, UK: 1982:48-58.
44. Mikhailov E, Vlasenko S, Niessner R, Pöschl U. Interaction of aerosol particles composed of protein and salts with water vapor: hygroscopic growth and microstructural rearrangement. *Atmos Chem Phys Discuss*. 2003;3(5):4755-4832.
45. Altman PL, Dittmer DS eds. *Respiration and Circulation*. Federation of American Societies for Experimental Biology; 1971.
46. Johnson GR, Morawska L. The mechanism of breath aerosol formation. *J Aerosol Med Pulm Drug Deliv*. 2009;22:229-237.
47. Morawska L, Johnson GR, Ristovski ZD, et al. Size distribution and sites of origin of droplets expelled from the human respiratory tract during expiratory activities. *J Aerosol Sci*. 2009;40:256-269.
48. Han ZY, Weng WG, Huang QY. Characterizations of particle size distribution of the droplets exhaled by sneeze. *J R Soc Interface*. 2013;10:20130560.
49. Graham DI, Moyeed RA. How many particles for my Lagrangian simulations? *Powder Technol*. 2002;125(2–3):179-186.
50. Wan MP, Sze To GN, Chao CYH, Fang L, Melikov A. Modeling the fate of expiratory aerosols and the associated infection risk in an aircraft cabin environment. *Aerosol Sci Technol*. 2009;43(4):322-343. doi:10.1080/02786820802641461
51. Fernandez MO, Thomas RJ, Garton NJ, Hudson A, Haddrell A, Reid JP. Assessing the airborne survival of bacteria in populations of aerosol droplets with a novel technology. *J R Soc Interface*. 2019;16:20180779. doi:10.1098/rsif.2018.0779
52. Anand S, Mayya YS. Size distribution of virus laden droplets from expiratory ejecta of infected subjects. *Sci Rep*. 2020;10(1):1-9.
53. Chen PZ, Bobrovitz N, Premji Z, Koopmans M, Fisman DN, Gu FX. Heterogeneity in transmissibility and shedding SARS-CoV-2 via droplets and aerosols. *eLife*. 2021;10:e65774.
54. Pöhlker ML, Krüger OO, Förster JD, et al. Respiratory aerosols and droplets in the transmission of infectious diseases. *arXiv*. 2021:2103.01188.
55. Jones RM. Relative contributions of transmission routes for covid-19 among healthcare personnel providing patient care. *J Occup Environ Hyg*. 2020;17(9):408-415.
56. Azimi P, Keshavarz Z, Laurent JGC, Stephens B, Allen JG. Mechanistic transmission modeling of covid-19 on the diamond princess cruise ship demonstrates the importance of aerosol transmission. *Proc Natl Acad Sci USA*. 2021;118(8):e2015482118.

How to cite this article: Coldrick S, Kelsey A, Ivings MJ, et al. Modeling and experimental study of dispersion and deposition of respiratory emissions with implications for disease transmission. *Indoor Air*. 2022;32:e13000. doi:10.1111/ina.13000